universe

IMPACT FACTOR 2.5

CITESCORE 4.3

Article

On the Classical Limit of Freely Falling Quantum Particles, Quantum Corrections and the Emergence of the Equivalence Principle

Juan A. Cañas, J. Bernal and A. Martín-Ruiz

MDPI

https://doi.org/10.3390/universe10090351

universe

MDPI

Article

On the Classical Limit of Freely Falling Quantum Particles, Quantum Corrections and the Emergence of the Equivalence Principle

Juan A. Cañas [1], J. Bernal [2] and A. Martín-Ruiz [1,*]

[1] Instituto de Ciencias Nucleares, Universidad Nacional Autónoma de México, Ciudad de México 04510, Coyoacán, Mexico; juan.canas@correo.nucleares.unam.mx
[2] División Académica de Ciencias Básicas, Universidad Juárez Autónoma de Tabasco, Cunduacán 86690, Tabasco, Mexico; jorge.bernal@dacb.ujat.mx
* Correspondence: alberto.martin@nucleares.unam.mx

Abstract: Quantum and classical mechanics are fundamentally different theories, but the correspondence principle states that quantum particles behave classically in the appropriate limit. For high-energy periodic quantum systems, the emergence of the classical description should be understood in a distributional sense, i.e., the quantum probability density approaches the classical distribution when the former is coarse-grained. Following a simple reformulation of this limit in the Fourier space, in this paper, we investigate the macroscopic behavior of freely falling quantum particles. To illustrate how the method works and to fix some ideas, we first successfully apply it to the case of a particle in a box. Next, we show that, for a particle bouncing under the gravity field, in the limit of a high quantum number, the leading term of the quantum distribution corresponds to the exact classical distribution plus sub-leading corrections, which we interpret as quantum corrections at the macroscopic level.

Keywords: classical limit; quantum bouncer; universality of free fall

Citation: Cañas, J.A.; Bernal, A.; Martín-Ruiz, A. On the Classical Limit of Freely Falling Quantum Particles, Quantum Corrections and the Emergence of the Equivalence Principle. *Universe* **2024**, *10*, 351. https://doi.org/10.3390/universe10090351

Academic Editor: Gerald B. Cleaver

Received: 20 July 2024
Revised: 21 August 2024
Accepted: 28 August 2024
Published: 2 September 2024

1. Introduction

In general, the correspondence principle states that the predictions of a new physical theory becomes identical to the predictions of an old theory in the appropriate limit. For example, the correspondence principle is accomplished by special relativity, which reduces to the Newtonian prediction for velocities much smaller than the speed of light in a vacuum. Also, the general theory of relativity reduces to the Newtonian gravitation for weak gravitational fields. In a similar fashion, one expects the predictions of quantum mechanics to reproduce those of classical mechanics in some limit; however, such quantum-to-classical correspondence is more subtle, such that there is no agreement after a century of discussion. The main difficulty is perhaps that the conceptual frameworks of these theories are fundamentally different. This led Einstein to assert, as subtly discussed in his famous letters with Born, that quantum formalism is inadequate for providing a complete description of reality [1].

In the literature, one can find various approaches to discussing the quantum-to-classical correspondence [2–6], all of them rooted in either (i) Planck's limit $h \to 0$ or (ii) Bohr's correspondence principle $n \gg 1$ [7]. The former was introduced to show that the Planck energy density for black-body radiation reduces to the Rayleigh–Jeans law as $h \to 0$, and the latter was introduced to show that the transition frequency between neighboring energy levels in the hydrogen atom tends to the classical orbital frequency of the electron as $n \gg 1$. As pointed out by Liboff, these two formulations are not universally equivalent [8]. On the other hand, since these statements of the correspondence principle were introduced before the development of modern quantum mechanics, it was not clear how they should be

applied to the wave function or matrix elements of an operator. Some methods addressing the quantum-to-classical correspondence in the context of modern quantum theory include the WKB method, the path integral formulation and Ehrenfest's theorem. In Ref. [9], we discussed in detail why these approaches are not universally reliable for investigating the classical limit of quantum mechanics, since, at the end, all of them require a very narrowly peaked probability density.

The quantum–classical correspondence has also been discussed using the Wigner phase-space formulation of quantum mechanics [10]. This seems to be a natural framework to tackle this problem since both theories can be expressed in terms of a joint position–momentum distribution. Indeed, as shown in Ref. [11] for a quantum harmonic oscillator, the classical limit of the Wigner function for highly excited states (i.e., coherent and WKB states) yields the microcanonical ensemble. Other important analyses of the quantum–classical correspondence in the framework of the Wigner function are presented in references [12–14].

On the other side, a simpler and often more intuitive approach for visualizing the quantum–classical correspondence in periodic systems involves a direct comparison of the probability densities in either position or momentum spaces [15–19]. Of course, such correspondence does not arise pointwise since the quantum distribution is highly oscillatory for $n \gg 1$ while the classical distribution is smooth between the turning points. Instead, as is widely accepted [8], the correspondence should be understood in a locally averaged sense. The analytical evaluation of local averages is rather difficult in the position space and it can be performed only for the infinite square well potential [15], whose quantum distribution is mathematically simple enough. This problem was invoked by Einstein to illustrate his concerns on the completeness of quantum mechanics, concluding that, despite the emergence of the classical distribution, it requires speaking of an ensemble and tells nothing on the individual particle [1]

In recent papers, we reformulated the method to evaluate the local average of a quantum distribution based on two reasonable simple assumptions: (i) the system is periodic and (ii) the quantum distribution rapidly oscillates for high quantum numbers around the classical distribution [20–22]. Periodicity allows us to express the classical and quantum distributions in Fourier series, and the local averaging process in position space implies that the quantum Fourier coefficient asymptotically approaches the classical Fourier coefficient. This simple procedure renders, at first order of approximation, the exact classical probability density for intricate periodic quantum systems, such as the nonrelativistic [20] and relativistic [23] harmonic oscillator, the hydrogen atom [22] and the quantum bouncer [9]. However, the analysis of the subdominant terms of the asymptotic distribution remains open. These terms, being nonvanishing, can be interpreted as a residual quantum behavior at the macroscopic scale. Physically, this means that the convergence in distribution does not produce the exact classical results but a macroscopic quantum distribution that consists of the classical distribution plus small oscillations around it. This analysis is far from trivial and, in this paper, we aim to fill this gap. In particular, we will focus on the quantum corrections to the quantum bouncer. As mentioned, in Ref. [9], we computed the exact classical limit of this system and envisaged the emergence of the quantum corrections, which were not discussed nor computed there. Here, we shall present a full theory to investigate the quantum corrections in general, which are to be applied to this particular system. We choose this system because, apart from its importance from the quantum–mechanical side (which implies that the macroscopic description of a system emerges from quantum mechanics), it also has profound implications from the gravitational point of view, as we shall discuss in the following.

The universality of free fall (UFF), often referred to as the weak equivalence principle, states that every test body (being small enough to neglect the effects of gravity gradients) experiences the same acceleration in a gravitational field, regardless of their mass or internal composition. It constitutes one of the logical foundations of general relativity [24]. The UFF also represents a profound difference between the classical and quantum domains since the

dynamics of quantum particles are mass-dependent and thus not satisfying the essence of the weak equivalence principle [25]. The validity of the UFF requires the Eötvös parameter to be zero for any couple of test bodies freely falling in the presence of a gravity field [26,27]. Classical and quantum experiments performed to constrain the value of this parameter have been reported, the former with an astonishing precision [27,28], highly overcoming that of the second ones [29–31], though there are proposals to dramatically improve the precision of quantum tests [32]. The validity of the UFF in quantum mechanics has also been studied theoretically, yielding many different conclusions by means of different approaches [33–35]. Other authors have discussed the relevance of this subject as well [36,37]. In this paper, we demonstrate that the UFF is an emergent phenomenon. Following the method that we introduced, we show that the macroscopic behavior of the quantum bouncer implies, at first order of approximation, the validity of the UFF. However, the quantum corrections indicate that, even at the macroscopic scale, there is a residual mass-dependent quantum–mechanical behavior, which implies that the UFF is not universal at all but an emergent phenomenon in the classical world.

The remainder of this paper is organized as follows. In Section 2, we introduce the method in a pedagogical fashion. For the sake of clarity, we first discuss what the classical probability density means and then we reformulate the local averages in the Fourier space. As a guiding model, in Section 3, we apply the method to the infinite square well potential. Next, in Section 4, we show that, for a particle bouncing under a gravity field, in the limit of a high quantum number, the leading term correctly reproduces the classical distribution. We discuss in detail the sub-leading terms, which are interpreted as quantum corrections. Finally, in Section 5, we summarize our results and provide some context for the relevance of our findings.

2. Emergence of a Macroscopic Description from Coarse-Grained Quantum Mechanics

In this section, we review the method that we developed in Refs. [20–22]. For a pedagogical introduction to the method, we first discuss the meaning of a classical probability distribution and present a formal definition in position representation. Next, assuming the coarse-grained convergence of the quantum distribution to the classical distribution in the limit of a high quantum number, we reformulate the method in the Fourier space and discuss some subtleties.

2.1. Classical Probability Density

The classical mechanics of a particle give deterministically the position and momentum as a function of time and hence we do not require a probabilistic description in this case. This is why we do not often discuss the concept of a classical probability function in the classical mechanics context. However, this concept is precisely what provides the bridge to investigate the quantum-to-classical transition, and hence deserves a detailed discussion.

For a consistent definition of the probability density within the classical physics, we need to introduce a randomness element into the problem. One possibility is by stipulating that the motion initiates at a random time or that the measurement occurs at a random time [16]. Another possibility is by assuming that we are dealing with a large number of identical systems, such that we cannot know the starting times for all these systems. Following these ideas, we shall formulate the concept of the classical probability density.

Let us consider a generic one-dimensional potential $V(x)$, as shown in Figure 1, which can give rise to bound states that can be described either classically or quantum mechanically. Since we are considering one-dimensional motion solely, the particle bounces back and forth between the classical turning points at x_a and x_b, with a period τ. The

turning points are defined, for a fixed value of energy E, as $V(x_a) = V(x_b) = E$, and the classical period is given by

$$\tau = \sqrt{2m} \int_{x_a}^{x_b} \frac{dx}{\sqrt{E - V(x)}}. \tag{1}$$

We now introduce the concept of the classical probability density, $\rho_{\rm cl}(x)$. We can easily define the classical probability $dP_{\rm cl} = \rho_{\rm cl}(x)dx$ as the probability of finding the particle in the interval $[x, x + dx]$ at a random time t. We note that each value of x will be realized twice per classical period, one each in the back/to and forth/from parts of the motion. Therefore, the probability $dP_{\rm cl}$ can be estimated as how much time $dt(x)$ the particle spends in the region $[x, x + dx]$ during one period τ. This simple argument gives

$$dP_{\rm cl} = \rho_{\rm cl}(x)dx = \frac{dt(x)}{\tau/2}, \tag{2}$$

where $\tau/2$ is half the classical period. From this expression, we read the properly normalized classical probability density as

$$\rho_{\rm cl}(x) = \frac{2}{\tau|v(x)|} = \frac{1}{\tau}\sqrt{\frac{2m}{E - V(x)}}, \tag{3}$$

where $v(x)$ is the local speed. Physically, this result implies that, if we perform a measurement at a random time, the particle is more likely measured at positions where it travels slowly. Since the classical motion is restricted between the turning points, $\rho_{\rm cl}(x) = 0$ for $x \notin (x_a, x_b)$. As anticipated, we shall use this simple formulation of the classical probability density to make contact with the quantum mechanical probability density $\rho_n^{\rm qm}(x)$, defined by

$$\rho_n^{\rm qm}(x) = \psi_n^*(x)\psi_n(x), \tag{4}$$

where $\psi_n(x)$ is an energy eigenstate of the system and n is the principal quantum number.

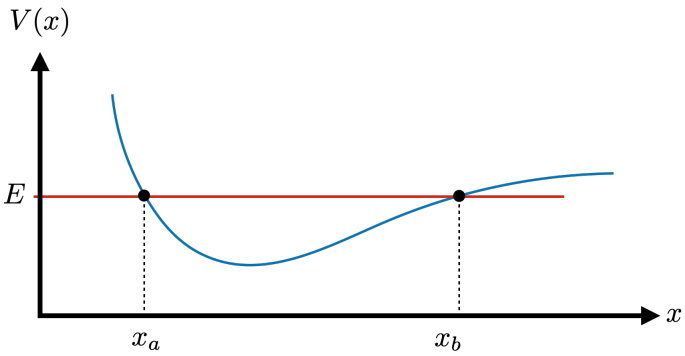

Figure 1. Plot of a generic one-dimensional potential $V(x)$ supporting bound-state motion (blue line). The red line indicates the value of the energy E, whose intersection with the potential $V(x)$ determines the turning points x_a and x_b, indicated with the vertical dashed-lines.

2.2. Local Average of the Quantum Probability Density

Many authors illustrate the validity of Bohr's correspondence principle by directly comparing the classical and quantum probability densities for large quantum numbers, as defined by Equations (3) and (4), respectively. These kinds of plots are quite common in the literature and can be found, for example, in Refs. [15–19] for simple bound-state systems, such as the particle in a box, the harmonic oscillator, the hydrogen atom and the quantum bouncer. Such plots reveal that the highly oscillatory quantum probability density $\rho_n^{\rm qm}(x)$ does not converge pointwise to the smooth classical probability density $\rho_{\rm cl}(x)$ in

any limit. Instead, the classical limit should be understood in a distributional sense, which means that, for every smooth function $f(x)$, the integral $\int f(x)\rho_n^{\rm qm}(x)dx$ must converge to $\int f(x)\rho_{\rm cl}(x)dx$. In this sense, any function $f(x)$ provides averaging over rapid oscillations of the quantum probability density and hence it is justified to speak about the classical limit. The notation to say that $\rho_n^{\rm qm}(x)$ converges in distribution to $\rho_{\rm cl}(x)$ is $\rho_n^{\rm qm}(x) \xrightarrow{d} \rho_{\rm cl}(x)$ [38,39]. The convergence in distribution means that the quantum distribution $\rho_n^{\rm qm}(x)$, if averaged locally in a finite interval, approaches the classical distribution $\rho_{\rm cl}(x)$ for sufficiently large values of the principal quantum number n. A more formal statement of this might be that

$$\rho_{\rm cl}(x) = \lim_{n\gg 1} \frac{1}{2\epsilon_n} \int_{x-\epsilon_n}^{x+\epsilon_n} \rho_n^{\rm qm}(y)\, dy, \tag{5}$$

where the interval ϵ_n decreases as the quantum number n increases [8]. As is, the formula (5) can be successfully applied to the case of a particle in a box [15]. However, it is impractical for more intricate bound-state systems, such as the harmonic oscillator, the hydrogen atom and the quantum bouncer. We now reformulate the Formula (5) in a different manner.

Since any periodic motion can be expressed as a superposition of sinusoidal harmonic modes, we can write a periodic function $f(\lambda)$, where λ can be the time t or a spatial coordinate x, as a series of sinusoidal functions, i.e., as a Fourier series [40]. The function f can be taken as either the classical and quantum probability densities for bound-state systems, for example. We then introduce the Fourier expansions:

$$\rho_{\rm cl}(x) = \frac{1}{2\pi\hbar}\int \rho_{\rm cl}(p)e^{ipx/\hbar}dp, \qquad \rho_n^{\rm qm}(x) = \frac{1}{2\pi\hbar}\int \rho_n^{\rm qm}(p)e^{ipx/\hbar}dp, \tag{6}$$

where $\rho_{\rm cl}(p)$ and $\rho_n^{\rm qm}(p)$ are the classical and quantum Fourier coefficients, respectively. Needless to say, the Fourier coefficient in Equation (6), $\rho_n^{\rm qm}(p)$, does not correspond to the momentum space probability density $|\phi_n(p)|^2$, where $\phi_n(p) = \frac{1}{2\pi\hbar}\int \psi_n(x)e^{-ipx/\hbar}dx$ is the wave function in momentum space. Instead, $\rho_n^{\rm qm}(p)$ has the same information content as the probability distributions in position space $\rho_n^{\rm qm}(x)$, just encoded in a different way.

Substitution of the Fourier expansions (6) into Equation (5) leads to

$$\int \rho_{\rm cl}(p)e^{ipx/\hbar}dp = \lim_{n\gg 1}\int \rho_n^{\rm qm}(p)\left[\frac{1}{2\epsilon_n}\int_{x-\epsilon_n}^{x+\epsilon_n} e^{ipy/\hbar}\, dy\right]dp. \tag{7}$$

Evaluating the inner integral and keeping only the leading ϵ_n-independent term, we obtain

$$\int \rho_{\rm cl}(p)e^{ipx/\hbar}dp \sim \lim_{n\gg 1}\int \rho_n^{\rm qm}(p)e^{ipx/\hbar}dp. \tag{8}$$

Finally, the linearity of the Fourier expansions implies, from Equation (8), that the quantum Fourier coefficient $\rho_n^{\rm qm}(p)$ approaches, asymptotically, the classical Fourier coefficient $\rho_{\rm cl}(p)$ for $n \gg 1$, i.e.,

$$\lim_{n\gg 1} \rho_n^{\rm qm}(p) \sim \rho_{\rm cl}(p) + \mathcal{O}(1/n). \tag{9}$$

This expression, expressed in the Fourier space, is equivalent to the local average process of Equation (5) in position space. We observe that, being n large, the quantum Fourier coefficient $\rho_n^{\rm qm}(q)$ will be expressed as a power series of $1/n$ such that the leading term will correspond exactly with the classical coefficient $\rho_{\rm cl}(q)$, and the higher-order terms will be quantum corrections at the macroscopic level. In previous papers, we have shown that the leading term correctly yields the classical distribution for different systems, such as the particle in a box and the harmonic oscillator [20], the hydrogen atom [22] and, much more recently, the quantum bouncer [9]. However, the quantum corrections have not received attention yet. Here, we aim to fill in this gap since it has important physical implications.

3. A Guiding Model: The Infinite Square Well Potential

Consider the simplest bound-state problem in quantum theory: a point particle in one dimension confined between perfectly reflecting walls at $x = 0$ and $x = L$. This potential, although simple, has been used to model real quantum well systems that can be created in the laboratory, e.g., it provides physical realizations of atomic mirrors [41]. Classically, the particle moves with the same speed v at every position inside the well because there are no forces acting there. Using the expression (3) for the classical probability density, with

$$V(x) = 0 \ \text{ for } \ x \in [0, L], \qquad E = \frac{1}{2}mv^2, \quad \text{and} \quad \tau = \frac{2L}{v}, \tag{10}$$

we obtain

$$\rho_{\rm cl}(x) = \frac{1}{L}\, H(x)H(L-x), \tag{11}$$

where $H(z)$ is the Heaviside step function defined by $H(z) = 1$ for $z \geq 0$ and $H(z) = 0$ for $z < 0$. Therefore, the classical probability density of finding the particle at x is constant inside the box and there is no preferable position for finding a classical particle. The quantum-mechanical problem is quite different. In this case, the normalized eigenfunctions $\psi_n(x)$ satisfying Dirichlet boundary conditions on the walls and energy eigenvalues E_n can be written as

$$\psi_n(x) = \sqrt{\frac{2}{L}}\sin\Big(\frac{n\pi x}{L}\Big)\, H(x)H(L-x), \quad E_n = \frac{p_n^2}{2m} = \frac{n^2\pi^2\hbar^2}{2mL^2}, \quad n = 1, 2, 3, \cdots. \tag{12}$$

In Figure 2, we plot the dimensionless classical probability density (11) and the dimensionless quantum probability density $\rho_n^{\rm qm}(x) = \psi_n^*(x)\psi_n(x)$ for the excited energy eigenstate with $n = 3$ and for a high-energy eigenstate with $n = 20$. The former case suggests that the probability of finding the particle near to the walls is nearly zero. Also, there are specific points, the nodes, in which the probability of finding the particle is zero. Clearly, this situation cannot be interpreted in terms of classical physics since it implies that the particle accelerates and decelerates continuously, even in the absence of forces inside the box. In the latter case, we observe that the classical distribution $\rho_{\rm cl}(x)$ does not follow the quantum distribution $\rho_n^{\rm qm}(x)$ but instead follows the local average. This can be understood as follows. In a high-energy eigenstate ($n \gg 1$), the wavelength is very short and hence, at every point inside the box, there are effectively a peak and a node. So, as n is increased, peaks and nodes get closer and closer to each other and the quantum distribution appears to become a constant equal to the average of the peak and the node, i.e., equal to $1/L$, which is the classical distribution, thus losing any information regarding the nodes, but this is indeed true only in the formal limit $n \to \infty$. This naive conclusion is reached when averaging over an oscillation solely, but this is not the case, since, as discussed in the previous section, the quantum-to-classical transition should be understood in a distributional sense, and hence information regarding the nodes must survive in the limiting process, as we shall see in the following. Now, let us derive this result in an analytical fashion by using the mathematical formulation introduced in Section 2.2. Fourier expanding the quantum probability density $\rho_n^{\rm qm}(x)$, as defined in Equation (6), gives the Fourier coefficients

$$\rho_n^{\rm qm}(p) = \int \rho_n^{\rm qm}(x)e^{-ipx/\hbar}dx = \frac{1}{iQ}\,\frac{1-e^{-iQ}}{1-\left(\frac{Q}{2\pi n}\right)^2}, \tag{13}$$

where $Q \equiv pL/\hbar \in (-\infty, +\infty)$. Of course, by inverse Fourier transforming this expression, we go back to the sinusoidal quantum probability density. Now, we look for the asymptotic

behavior of the Fourier coefficient (13) in the limit $n \gg 1$. We have to carry this out with some care. For large n, this expression can be written as the geometric series

$$\rho_n^{\rm qm}(p) \sim \frac{1}{iQ}\left(1-e^{-iQ}\right)\sum_{k=0}^{\infty}\left(\frac{Q}{2\pi n}\right)^{2k}, \tag{14}$$

which is valid over the compact domain $|Q| < 2\pi n$ in order to guarantee its convergence. This imposes a restriction upon the Fourier variable p, namely $|p| < 2p_n$, where $p_n = n\pi\hbar/L$ is the momentum defined by Equation (12). This restriction, which emerges from the mathematical structure of the quantum Fourier coefficient, is indeed physical since it is also consistent with the condition imposed by the energy surface in the classical case. Therefore, though in the quantum regime the momentum can reach any value, once we fix the (high) energy of the system to obtain the asymptotic behavior of the Fourier coefficient for $n \gg 1$, the possible values for the momentum become restricted. This subtle fact was not considered in Ref. [20] and we shall explore its consequences in the following.

Keeping the leading order terms up to $1/n^2$ in Equation (14), we obtain

$$\rho_n^{\rm qm}(q) \sim \frac{1}{iQ}\left(1-e^{-iQ}\right)\left[1+\left(\frac{Q}{2\pi n}\right)^2+\mathcal{O}(1/n^4)\right], \tag{15}$$

for $|Q| < 2\pi n$. Therefore, the asymptotic behavior of the quantum probability density in position space is obtained by Fourier transforming Equation (15) as defined in Equation (6). We obtain

$$\rho_n^{\rm qm}(x) \sim \frac{1}{2\pi\hbar}\int \rho_n^{\rm qm}(p)e^{ipx/\hbar}dp = \frac{1}{2\pi L}\int_{-2n\pi}^{+2n\pi}\frac{1-e^{-iQ}}{2\pi iQ}\left[1+\left(\frac{Q}{2\pi n}\right)^2\right]e^{iQ\chi}\,dQ, \tag{16}$$

where $\chi \equiv x/L$. This integral is quite simple. The result is

$$\begin{aligned}\rho_n^{\rm qm}(x) \sim & \frac{1}{L}\frac{{\rm Si}[2n\pi(1-\chi)]+{\rm Si}(2n\pi\chi)}{\pi} \\ & + \frac{1}{Ln^2}\frac{(1-2\chi)\sin(2\pi n\chi)+2\pi n\chi(\chi-1)\cos(2\pi n\chi)}{4\pi^3(\chi-1)^2\chi^2},\end{aligned} \tag{17}$$

where Si is the sine integral, defined as ${\rm Si}(x) = \int_0^x \frac{\sin t}{t}dt$. Note that, in Equation (17), x is not restricted to being between 0 and L, as in the original classical and quantum distributions. In Figure 3, we plot the asymptotic distribution (17) for different values of n. Taking $n = 10$, we can see that the macroscopic distribution $\rho_{10}^{\rm qm}(x)$ exhibits oscillations around the classical distribution inside the quantum well and around zero outside. As we increase n, for example, up to $n = 30$, the amplitude of the oscillations decreases in both regions. As discussed above, in the formal limit $n \to \infty$, we obtain a smooth distribution, i.e., without the small oscillations. This can be seen by using the asymptotic expansion $\lim_{n\gg 1}{\rm Si}(2n\pi x) \sim \frac{\pi}{2}{\rm sign}(x) - \frac{\cos(2n\pi x)}{2n\pi x} + \mathcal{O}(n^{-2})$ [42], such that the limit $n \to \infty$ upon Equation (17) produces

$$\lim_{n\to\infty}\rho_n^{\rm qm}(x) = \rho_{\rm cl}(x) = \frac{1}{L}\,H(x)H(L-x), \tag{18}$$

which is exactly the smooth classical probability density. Note that the oscillatory behavior of the macroscopic distribution vanishes only in the formal limit $n \to \infty$. In a realistic classical situation, the value of n is given by $n = \sqrt{E_{\rm cl}/E_1} = \sqrt{p_{\rm cl}/p_1}$, where $E_{\rm cl}$ ($p_{\rm cl}$) is the classical energy (momentum), and hence the small oscillations around the classical distribution survive. For example, for a thermal Neutron with $E_{\rm cl} \approx 10^{-21}$J trapped in a 1 mm box, we obtain $n \approx 10^7$. For the even more classical case of a particle with mass 1 g moving at 1m/s inside a 1 cm box, one obtains $n \approx 10^{28}$. Therefore, the small quantum

oscillations that we can see in Figure 3 are due to the small values of n that we are using there compared with the realistic value of 10^{28}. Therefore, macroscopically, such oscillations are strongly suppressed.

As a consistency check, let us evaluate the expectation value of x^k by using the classical, quantum and asymptotic probability densities. The classical expectation value is a simple task, with the result $\langle x^k \rangle_{\rm cl} = \int \rho_{\rm cl}(x)\, x^k\, dx = L^k/(k+1)$. The quantum expectation value can also be computed in a closed form, and it can be expressed in terms of the generalized hypergeometric function ${}_1F_2(a;b,c;z)$ as

$$\begin{aligned}\langle x^k \rangle_n^{\rm qm} &= \int \rho_n^{\rm qm}(x)\, x^k\, dx \\ &= -(\pi n)^2 L^k\, \Gamma(3/2)\, \Gamma[(k+1)/2]\; {}_1F_2\left[\frac{k+3}{2}; \frac{3}{2}, \frac{k+5}{2}; -(n\pi)^2\right]. \end{aligned} \tag{19}$$

For the sake of comparison, we now evaluate the expectation value by using the asymptotic distribution (17). Keeping terms up to order $1/n^2$, we obtain

$$\langle x^k \rangle_n^{\rm qm} \sim \langle x^k \rangle_{\rm cl} \left[1 - \frac{k(k+1)}{4\pi^2 n^2}(1 - \delta_{k1})\right], \tag{20}$$

and this result can also be obtained by power expanding the exact quantum result (19) in inverse powers of the quantum number n. Once again, one can further see that the formal limit $n \to \infty$ applied on Equation (20) yields the exact classical result. In a realistic case, the additional term in Equation (20) is present and can be interpreted as a residual quantum behavior at the macroscopic level.

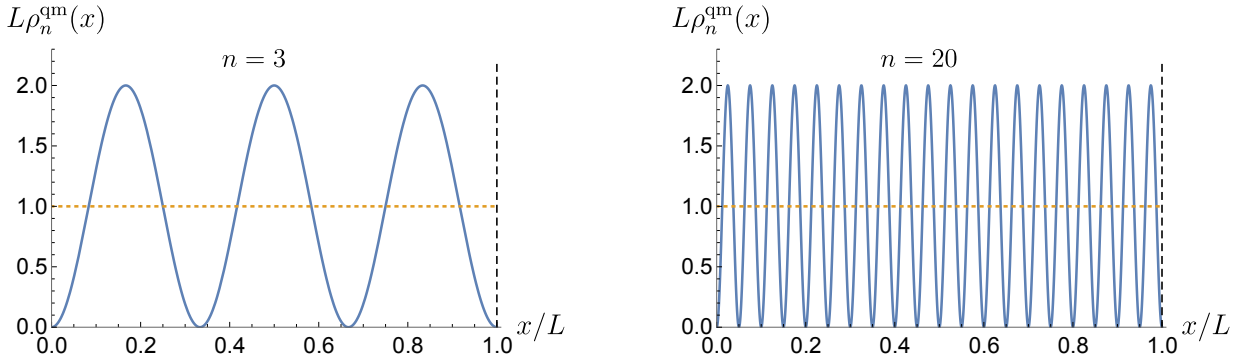

Figure 2. Dimensionless quantum probability density (blue continuous line) $L\rho_n^{\rm qm}(x)$ of the particle in a box for different values of the quantum number n. The yellow dotted lines correspond to the (dimensionless) classical probability density $L\rho_{\rm cl}(x)$.

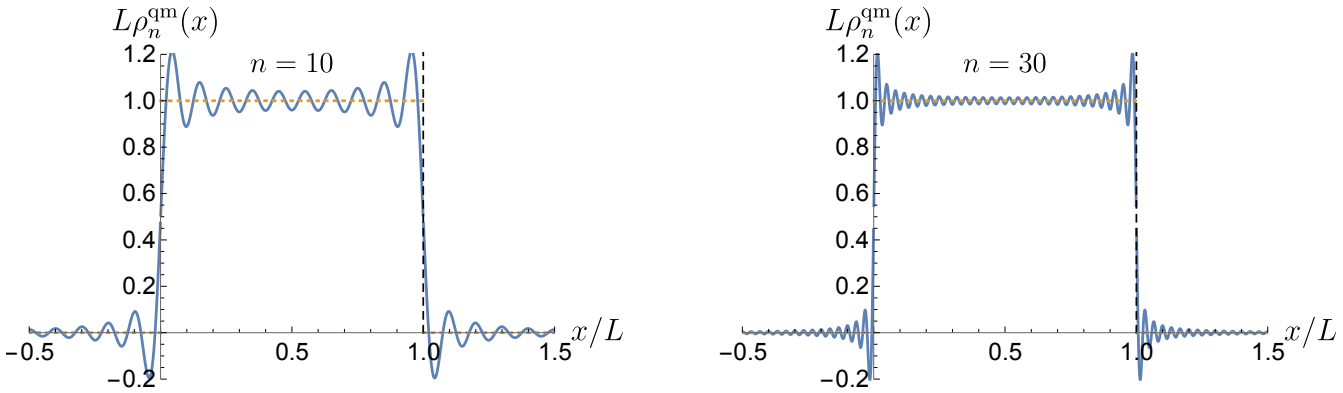

Figure 3. (Dimensionless) classical (horizontal yellow line) and quantum (oscillatory blue line) probability densities for a high-energy eigenstate with $n = 20$.

4. The Quantum Bouncer: Exact Result and Quantum Corrections

The quantum bouncer, which is the problem of a particle bouncing on a perfectly reflecting surface under the influence of gravity, is described by a constant field force with the appropriate boundary condition at the ground level [43]. Strikingly, the GRANIT experiment conducted at the Institute Laue-Langevin [44] and the qBOUNCE collaboration [45] have observed the gravitational quantum states of ultracold neutrons bounded by the Earth's gravitational field. In these experiments, neutrons do not bounce smoothly but at certain well-defined quantized heights, in agreement with the predictions of quantum mechanics. UCNs bridge the gap between gravity experiments at short distances and the precise measurement techniques of quantum mechanics. Due to this, they have been used to perform weak equivalence principle tests as well as probing the Newton's inverse square law of gravity at short distances [45,46].

All the basics of the quantum bouncer were introduced in Ref. [9]. Here, we just summarize the required results in the presence of the linearized potential energy

$$V(z) = \begin{cases} mgz & z > 0 \\ \infty & z \leq 0 \end{cases}, \tag{21}$$

where g is the gravitational acceleration, m is the gravitational mass and the vertical position z is measured from the ground level $z = 0$. Assuming that the particle is initially at rest and dropped from a height h, the classical probability density is found to be

$$\rho_{\rm cl}(z) = \frac{1}{2\sqrt{h(h-z)}} H(h-z)\, H(z). \tag{22}$$

Clearly, the probability density blows up as $z \to h$ since the particle spends a relatively longer time near h. It is worth pointing out that the function $\rho_{\rm cl}(z)$ does not depend on the mass of the particle, in contrast with the expressions for the classical distributions for the harmonic oscillator [20] and the hydrogen atom [22]. This is a direct consequence of the universality of free fall, often referred to as the weak equivalence principle, which is exactly true in classical mechanics.

The associated quantum mechanical problem, the so-called quantum bouncer, is more intricate. The normalized solution to the Schrödinger equation that satisfies the boundary condition $\psi_n(z = 0) = 0$ (i.e., the ground is impenetrable) and decays as z goes to infinity is [47–49]

$$\psi_n(z) = \frac{1}{\sqrt{l_g}} \frac{{\rm Ai}(a_n + z/l_g)}{{\rm Ai}'(a_n)}, \tag{23}$$

where ${\rm Ai}(x)$ is the Airy function [50], a_n is the n-th zero of the Airy function ${\rm Ai}(x)$ and $l_g = \left(\frac{\hbar^2}{2m^2 g}\right)^{1/3}$ is the gravitational length. The resulting quantized energies are given by $E_n = -mgl_g a_n$ with $n = 1, 2, 3, \cdots$.

In Figure 4, we superimpose the normalized quantum probability density $h_n \rho_n^{\rm qm}(z) = h_n |\psi_n(z)|^2$ (continuous blue line) with the normalized classical distribution $h_n \rho_{\rm cl}(z)$ (dashed yellow line) as a function of the normalized distance z/h_n and for different values of n, namely for the ground state $n = 1$ and for the excited state with $n = 20$. Here, $h_n = -l_g a_n$ determines the turning point. As in the case of the infinite square well potential, the quantum probability density for the n-th eigenstate rapidly oscillates around the smooth classical distribution for $n \gg 1$.

We now proceed to the evaluation of the Fourier coefficient $\rho_n^{\rm qm}(p)$, which is given by

$$\rho_n^{\rm qm}(p) = \int \rho_n^{\rm qm}(z) e^{-ipz/\hbar} dz = \frac{1}{l_g\, {\rm Ai}'^2(a_n)} \int_0^\infty {\rm Ai}^2(a_n + z/l_g)\, e^{-ipz/\hbar} dz. \tag{24}$$

As far as we know, the exact analytical evaluation of this integral has not been reported yet. However, for the purposes of this paper, we only require its asymptotic behavior for $n \gg 1$. To achieve this, we use the method of Albright [50], as some basic primitives of the Airy functions allow us to express the Fourier coefficient (24) as a series in inverse powers of a_n. The details of the calculations are relegated to Appendix A, and here we only present the final results. Let us only retain the dominant terms. For the sake of simplicity, we split the Fourier coefficient (24) as the sum of two terms, i.e., $\rho_n^{\rm qm}(p) \sim \rho_n^{(0)}(p) + \rho_n^{(1)}(p)$. The leading term $\rho_n^{(0)}(p)$ is found to be

$$\rho_n^{(0)}(p) = e^{-iQ_n} \sqrt{\frac{\pi}{2Q_n}} \frac{1+i}{2} \operatorname{erf}\left(\frac{1-i}{\sqrt{2}} \sqrt{Q_n} \right), \tag{25}$$

where $Q_n \equiv p h_n/\hbar$, and $\operatorname{erf}(x)$ is the error function defined by Equation (A11) [42]. The sub-leading term is given by

$$\rho_n^{(1)}(p) = \frac{1}{96 a_n^3} \left[-\left(15 - 8iQ_n^3\right) \rho_n^{(0)}(p) + 2Q_n(2Q_n + 5i) - 15 \right]. \tag{26}$$

Now, we have to inverse Fourier transform these coefficients to obtain the asymptotic form of the quantum probability density in position space. It can also be written as the sum of two terms, namely $\rho_n^{\rm qm}(z) \sim \rho_n^{(0)}(z) + \rho_n^{(1)}(z)$, where $\rho_n^{(0)}(z)$ and $\rho_n^{(1)}(z)$ are the Fourier transformations of Equations (25) and (26), respectively. To perform this, we have to take some care, since while the exact Fourier coefficient (24) is valid for $p \in (-\infty, \infty)$, the approximate expressions (25) and (26) are not. This situation is similar to the case of the Fourier coefficient for the infinite square well potential: while the exact coefficient (13) is valid for $Q \in (-\infty, +\infty)$, the asymptotic coefficient (15) is valid for $|Q| < 2\pi n$. To clearly see this point, one can inverse Fourier transform the leading order term (25) over $p \in (-\infty, \infty)$ and obtain the exact classical result

$$\rho_n^{(0)}(z) = \frac{1}{2\pi\hbar} \int_{-\infty}^{\infty} \rho_n^{(0)}(p)\, e^{ipz/\hbar}\, dp = \frac{H(h_n - z)\, H(z)}{2\sqrt{h_n(h_n - z)}}. \tag{27}$$

However, if the sub-leading term (26) is Fourier-transformed in a similar fashion, the corresponding integral does not converge. This is not surprising at all since, as discussed, the application of the method of Albright to compute the asymptotics of the quantum Fourier coefficient (24) has a definite domain of validity, something like what happens with the infinite square well potential. Recall that, in order to properly obtain an expansion of the quantum Fourier coefficient (13), we restricted the Fourier variable p to the domain $p \in [-2p_n, 2p_n]$, where $p_n = n\pi\hbar/L$ is the momentum of the particle. In the quantum bouncer case, we have a similar situation, since our expression for the Fourier coefficient is valid over a finite domain solely, since we truncate the series when using the method of Albright. Such analysis is still absent in the literature and we estimate it from a numerical analysis in Appendix B. Indeed, numerically, we determine the domain over the Fourier variable $Q_n = p h_n/\hbar$ to be $Q_n \in [a_n/2, -a_n/2]$, where a_n is the n-th zero of the Airy function. We are now ready to evaluate the inverse Fourier transform, which should be performed over the finite interval $p \in [-\hbar/2l_g, \hbar/2l_g]$. To keep close contact with the exact classical limit, we express the integral as follows $\int_{-\hbar/2l_g}^{\hbar/2l_g} = \int_{-\infty}^{\infty} - \int_{-\infty}^{-\hbar/2l_g} - \int_{\hbar/2l_g}^{\infty}$ and use the identity $\rho_n^{(0)}(-p) = [\rho_n^{(0)}(p)]^*$ such that

$$\begin{aligned} \rho_n^{(0)}(z) =& \frac{1}{2\pi\hbar} \int_{-\hbar/2l_g}^{\hbar/2l_g} \rho_n^{(0)}(p)\, e^{ipz/\hbar}\, dp \\ =& \frac{H(h_n - z)\, H(z)}{2\sqrt{h_n(h_n - z)}} - \frac{1}{\pi\hbar} \int_{\hbar/2l_g}^{\infty} \operatorname{Re}\left[\rho_n^{(0)}(p)\, e^{ipz/\hbar} \right] dp. \end{aligned} \tag{28}$$

The last integral can be approximated as follows. First, we take the real part explicitly:

$$\frac{1}{\pi\hbar}\int_{\hbar/2l_g}^{\infty}\mathrm{Re}\left[\rho_n^{(0)}(p)\,e^{ipz/\hbar}\right]dp=\frac{1}{\sqrt{2\pi}h_n}\int_{\lambda_n}^{\infty}\Big\{\cos[x(\zeta-1)]\,C(\sqrt{\pi x/2}) - \sin[x(\zeta-1)]\,S(\sqrt{\pi x/2})\Big\}\,\frac{dx}{\sqrt{x}}, \tag{29}$$

where $\lambda_n=-a_n/2>0$, $\zeta=z/h_n$ and $C(x)=\int_0^x\cos\left(\frac{\pi}{2}t^2\right)dt$ and $S(x)=\int_0^x\sin\left(\frac{\pi}{2}t^2\right)dt$ are the Fresnel integrals.

Now, for $n\gg1$, the integrand is highly oscillatory. In addition, the interval of integration (for large x) give us a way to approximate the integral since one can consider the asymptotic behavior of the Fresnel integrals for large arguments. Keeping the leading contribution, we obtain

$$\frac{1}{\pi\hbar}\int_{2\hbar/l_g}^{\infty}\mathrm{Re}\left[\rho_n^{(0)}(p)\,e^{ipz/\hbar}\right]dp\sim\frac{1}{2\sqrt{2\pi}h_n}\int_{\lambda_n}^{\infty}\frac{\cos[x(\zeta-1)]-\sin[x(\zeta-1)]}{\sqrt{x}}dx = \frac{H(h_n-z)\,H(z)}{2\sqrt{h_n(h_n-z)}}\left[1-\mathrm{C}\left(\sqrt{\frac{2\lambda_n}{\pi}(1-\zeta)}\right)-\mathrm{S}\left(\sqrt{\frac{2\lambda_n}{\pi}(1-\zeta)}\right)\right], \tag{30}$$

and therefore

$$\rho_n^{(0)}(z)=\frac{H(h_n-z)\,H(z)}{2\sqrt{h_n(h_n-z)}}\left[C\left(\sqrt{\frac{2\lambda_n}{\pi}(1-\zeta)}\right)+S\left(\sqrt{\frac{2\lambda_n}{\pi}(1-\zeta)}\right)\right]. \tag{31}$$

This expression gives the exact classical probability density with small oscillations around it. This is clearly seen from the asymptotic behavior of the Fresnel integrals for large arguments, i.e., $C(x)+S(x)\approx1+\frac{1}{\pi x}\left[\sin(\pi x^2/2)+\cos(\pi x^2/2)\right]$ for $x\gg1$. As in the quantum well case, the formal limit $n\to\infty$ yields the exact smooth classical probability distribution $\rho_{\mathrm{cl}}(z)$, given by Equation (22). Finite values of n retain the small oscillations, which we interpret as a residual quantum behavior at the macroscopic scale.

In all of the above, we have taken $n\gg1$ for definiteness and made some important approximations based on this assumption. Now, we shall better justify our choice. For a particle freely falling from a height h, the principal quantum can be estimated from $a_n=-h/l_g$. Since we are assuming that $n\gg1$, one can use the approximate expression for the zeros of the Airy function $a_n\approx-[(3\pi/2)(n-1/4)]^{2/3}$ and therefore $n\sim\frac{2}{3\pi}(h/l_g)^{3/2}$. For reference, for a Cs atom, one finds $l_g=0.226$ μm such that, if released from 1 mm, the corresponding quantum number is $n\sim62{,}500$. For the much lighter Na atom, one finds $l_g=0.727$ μm, which produces $n\sim10{,}000$. To obtain smaller values for n, the gravitational length must be larger, and this is achieved with lighter particles. For example, the gravitational length for a neutron is $l_g=5.87$ μm, which leads to $n\sim470$. These estimations justify our analysis of the above.

So far, we have studied only the physics arising from the leading order term of the quantum Fourier coefficient and showed the emergence of the exact classical probability distribution plus small quantum corrections with an amplitude driven by $\sim\lambda_n^{-1/2}\approx n^{-1/3}\ll1$. Now, we have to investigate the sub-leading term arising from the quantum Fourier coefficient $\rho_n^{(1)}(p)$ given by Equation (26). In addition, since the quantum correction arising from $\rho_n^{(0)}(p)$ decays as $n^{-1/3}$, we will keep terms up to this order in the following. The inverse Fourier transformation of Equation (26) then reads as

$$\rho_n^{(1)}(z) = \frac{1}{2\pi\hbar}\int_{-\hbar/2l_g}^{\hbar/2l_g} \rho_n^{(1)}(p) e^{ipz/\hbar} dp$$

$$\approx \frac{1}{192\pi h_n a_n^3}\int_{-\lambda_n}^{\lambda_n} \left[8iQ_n^3\,\rho_n^{(0)}(p) + 2Q_n(2Q_n+5i) - 15\right] e^{iQ_n\zeta}\, dQ_n, \tag{32}$$

where we have neglected the term decaying as $1/n^2$. Retaining the most important contributions, we obtain

$$\rho_n^{(1)}(z) \sim -\frac{1}{192\pi h_n}\frac{\sin(\zeta\lambda_n)}{\zeta\lambda_n}, \tag{33}$$

which decays as $n^{-2/3}$, i.e., faster than the correction arising in Equation (31). However, it is worth to mention that this term provides small oscillations beyond the classical turning point, which do not arise in Equation (31).

All of the above tell us that the asymptotic form of the quantum probability density in position space is

$$\rho_n^{\rm qm}(z) \sim \frac{H(h_n - z)\,H(z)}{2\sqrt{h_n(h_n-z)}}\left[1 + \frac{\sin[\lambda_n(1-\zeta)] - \cos[\lambda_n(1-\zeta)]}{\sqrt{2\pi\lambda_n(1-\zeta)}}\right] - \frac{1}{192\pi h_n}\frac{\sin(\zeta\lambda_n)}{\zeta\lambda_n}, \tag{34}$$

where we have power-expanded the Fresnel integrals in Equation (30) up to the first-order correction. The next-order expansion is smaller than those of Equation (33). In Figure 5, we plot the asymptotic distribution (34) for $n = 20$ (left panel) and $n = 100$ (right panel). We observe that the asymptotic distribution exhibits small oscillations around the smooth classical probability density. In these cases, the small oscillations are observable due to the small value of n that we are using, but they are strongly suppressed in a realistic situation.

To validate our results, we now evaluate some expectation values. For example, the classical expectation value of z^k, with $k \in \mathbb{Z}^+$, is

$$\langle z^k\rangle_{\rm cl} = \int_0^h z^k\,\rho_{\rm cl}(z)\,dz = h^k\,\frac{\sqrt{\pi}\,\Gamma(k+1)}{2\,\Gamma\left(k+\frac{3}{2}\right)}. \tag{35}$$

The expectation value can be computed easily by using the asymptotic probability density $\rho_n^{\rm qm}(z) \approx \rho_n^{(0)}(z) + \rho_n^{(1)}(z)$. Using the standard procedure to regularize infinite trigonometric integrals, we obtain

$$\langle z^k\rangle_n^{\rm qm} \sim \langle z^k\rangle_{\rm cl} + \frac{1}{2\pi\hbar}\int dp\,\rho_n^{(1)}(p)\lim_{\epsilon\to 0^+}\int_0^\infty z^k\,e^{ipz/\hbar}e^{-\epsilon z}\,dz$$

$$= \langle z^k\rangle_{\rm cl} + \frac{1}{2\pi\hbar}\int \rho_n^{(1)}(p)\frac{\Gamma(k+1)}{(-ip/\hbar)^{k+1}}dp, \tag{36}$$

such that the final result becomes

$$\langle z^k\rangle_n^{\rm qm} = \langle z^k\rangle_{\rm cl}\left[1 + \frac{-4k^3+6k^2+k+6}{48\,a_n^3}\right]. \tag{37}$$

Clearly, the second term can be interpreted as a quantum correction at the macroscopic level. For the sake of comparison, we have to evaluate the quantum expectation value and then power-expand the result up to a_n^{-3}. To our knowledge, a closed-form expression for

the quantum expectation value has not been reported yet. However, with the method of Albright, we can obtain an asymptotic expression for the expectation value, i.e.,

$$\langle z^k \rangle_n^{\rm qm} = \int_0^\infty z^k \rho_n^{\rm qm}(z)\, dz = \frac{l_g^k}{{\rm Ai}'^2(a_n)} \sum_{l=0}^{k} \binom{k}{l} (-a_n)^{k-l} \int_{a_n}^\infty x^l\, {\rm Ai}^2(x)\, dx$$

$$\sim h_n^k \sum_{l=0}^{k} \binom{k}{l} \frac{(-1)^l}{2l+1} \left[1 + \frac{l(l-1)(l-2)}{2(2l+1)(2l-5)} \frac{1}{a_n^3}\right], \tag{38}$$

and, performing the summations, we retrieve exactly the asymptotic expectation value given by Equation (37).

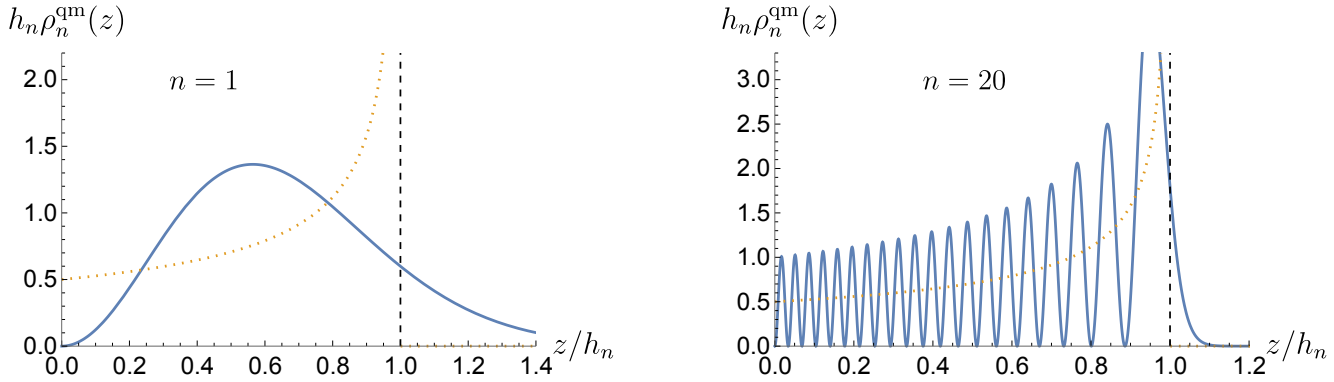

Figure 4. (Dimensionless) classical (horizontal yellow line) and quantum (oscillatory blue line) probability densities for the quantum bouncer for the ground state ($n = 1$) and for the excited state with $n = 20$.

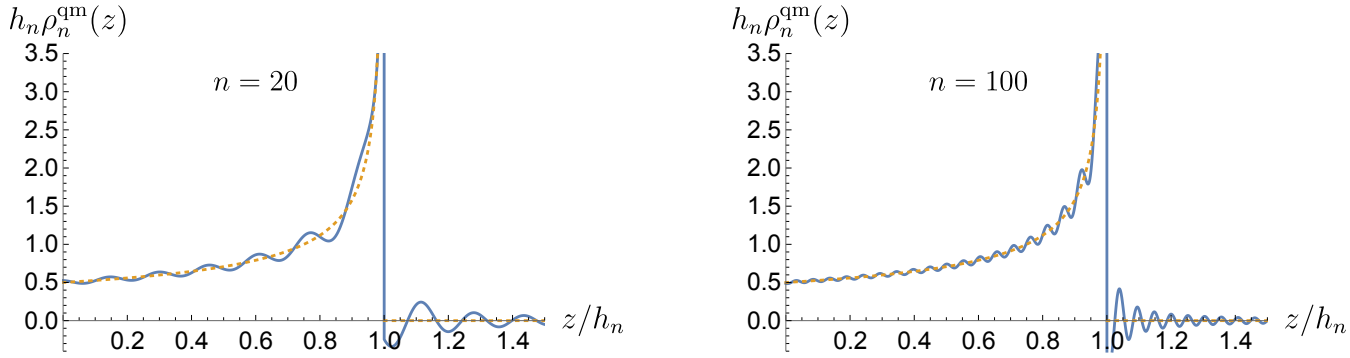

Figure 5. (Dimensionless) classical (horizontal yellow line) and quantum (oscillatory blue line) probability densities for a high-energy eigenstate with $n = 20$ and $n = 100$.

5. Conclusions

Classical and quantum descriptions of single-particle systems are fundamentally different: while the former tells us the exact position and momentum of a particle, the latter gives us the probability of finding the particle at some position or bearing some momentum. This makes the analysis of the quantum–classical correspondence difficult. There are traditional methods that address such correspondence, for example, the WKB method and the Ehrenfest's theorem; however, these are not universally reliable for investigating the classical limit in a general way. Also, the correspondence has been discussed in the language of the theory of distributions. By direct comparison of the classical and quantum probability densities, one realizes that the classical behavior emerges as a coarse-grained description of the quantum system. Therefore, since the correspondence is not pointwise, one expects the emergence of remnants of the quantum behavior at the macroscopic level as small oscillations enveloping the classical distribution.

The distributional quantum-to-classical convergence means that the quantum distribution, if averaged locally over a finite interval, approaches the classical distribution provided that the quantum number is large. This is formally expressed by Equation (5). The evaluation of Equation (5) is impractical in most cases (except for the infinite square well potential, since the quantum distribution is sinusoidal); however, it can be carried out in a simpler fashion when transformed to the Fourier space. In short, the convergence in distribution (5) is expressed in Fourier space by Equation (9), i.e., the quantum Fourier coefficient approaches the classical Fourier coefficient when the quantum number is large, but sub-leading quantum corrections emerge. In order to demonstrate the applicability of this method, we initially addressed the problem of a particle in a box. To this end, we compute an exact quantum Fourier coefficient (13), which is valid for any value of the momentum (Fourier variable), and then compute its asymptotic behavior for $n \gg 1$, which naturally restricts the domain of the Fourier variable (which, in this case, is dictated by the convergence of a geometric series). Finally, by inverse Fourier transforming the asymptotic quantum Fourier coefficient, we obtain Equation (17), which is the emergent macroscopic distribution in position space, i.e., the locally averaged quantum distribution. Figure 3 shows the macroscopic distribution. As expected, it behaves as the classical distribution plus small oscillations whose amplitude decreases as $1/n^2$ with $n \gg 1$. As a consistency check, we evaluated the exact expectation value of x^k (with $k \geq 0$) and demonstrated its consistency with the one computed when evaluated by using the macroscopic distribution. Our result implies that, at the macroscopic scale, all happens as if the quantum behavior is hidden, leaving us with an apparent world described consistently in a classical language.

The validity of the universality of free fall is one of the cornerstones of general relativity and one may ask if it emerges or not from the quantum behavior at high energies. Its validity in the classical domain is widely accepted, but the mass-dependent quantum dynamics explicitly break it. All of these factors motivate the analysis of the macroscopic behavior of the quantum bouncer: a particle bouncing on a perfectly reflecting surface under the influence of gravity. In this paper, we have also studied this problem following the program described above. The first step is the computation of the exact quantum Fourier coefficient (24). The integral cannot be evaluated in an analytical fashion. However, using the method of Albright, we obtained an asymptotic expression for $n \gg 1$, whose leading and sub-leading terms are given by Equations (25) and (26), respectively. The validity of these expressions was verified by comparing the asymptotics of the quantum Fourier coefficient (25) + (26) versus the exact result (24) computed numerically. This analysis also gave the domain of validity of our expansion. Finally, by inverse Fourier transforming the Fourier coefficient in the corresponding compact domain, we obtained the macroscopic distribution, given by Equation (34). In Figure 5, we superimposed the smooth classical distribution with our macroscopic distribution and reach similar conclusions as those of the particle in a box: for $n \gg 1$, the macroscopic distribution behaves as the classical distribution plus small oscillations, which we interpret as quantum corrections at the macroscopic level. All in all, our results indicate that the universality of free fall is an emergent phenomenon since quantum mechanics imply a remnant mass-dependent quantum behavior even at macroscopic scales.

We close by commenting on a possible generalization of this work. As discussed, the Wigner phase-space formulation of quantum mechanics provides a natural framework in which the quantum–classical correspondence can be studied in a common language: joint position–momentum distributions. The method that we introduced works in the position space, where one can directly visualize the distributional convergence of the probability densities. However, it is natural to wonder whether such a procedure can be extended to the phase-space probability distribution. We have left this problem for a future investigation.

Author Contributions: Conceptualization, J.A.C., A.M.-R. and J.B.; methodology, J.A.C., A.M.-R. and J.B.; investigation, J.A.C., A.M.-R. and J.B.; writing—original draft preparation, J.A.C., A.M.-R. and J.B.; writing—review and editing, J.A.C., A.M.-R. and J.B. All authors have read and agreed to the published version of the manuscript.

Funding: J.A.C. was supported by the CONAHCyT PhD fellowship No. 933498. A.M.-R. has been partially supported by DGAPA-UNAM Project No. AG100224 and by Project CONAHCyT (México) No. 428214.

Data Availability Statement: All data generated or analyzed during this study are included in this published article.

Acknowledgments: We acknowledge inspiring and useful discussions with Alejandro Frank and Andrea Valdés.

Conflicts of Interest: The authors of this manuscript declare no conflicts of interest.

Appendix A. Evaluation of the Fourier Coefficient for the Quantum Bouncer

The goal of this section is to obtain an approximate expression for the Fourier coefficient (24) in inverse powers of a_n for n large. To this end, in Equation (24), we first change variable to $x = a_n + z/l_g$ and then Taylor expand the exponential $e^{-ipx/\hbar} = \sum_{k=0}^{\infty} \frac{1}{k!}(-ipx/\hbar)^k$, i.e.,

$$\begin{aligned}\rho_n^{\rm qm}(p) &= \frac{e^{-iph_n/\hbar}}{{\rm Ai}'^2(a_n)} \int_{a_n}^{\infty} {\rm Ai}^2(x)\, e^{-ipl_g x/\hbar} dx \\ &= \frac{e^{-iph_n/\hbar}}{{\rm Ai}'^2(a_n)} \sum_{k=0}^{\infty} \frac{(-ipl_g/\hbar)^k}{k!} \int_{a_n}^{\infty} x^k\, {\rm Ai}^2(x)\, dx. \end{aligned} \tag{A1}$$

To evaluate this integral, we use the method of Albright. Indeed, if $A(x)$ and $B(x)$ are any two linear combinations of the Airy functions ${\rm Ai}(x)$ and ${\rm Bi}(x)$, and k a positive integer, the following recursive indefinite integral is valid [50]:

$$\begin{aligned}\int x^k A(x)B(x)dx &= \frac{x^{k+1}A(x)B(x)}{2k+1} - \frac{k(k-1)x^{k-2}A(x)B(x)}{2(2k+1)} \\ &\quad + \frac{kx^{k-1}[A(x)B'(x) + A'(x)B(x)]}{2(2k+1)} - \frac{x^k A'(x)B'(x)}{2k+1} \\ &\quad + \frac{k(k-1)(k-2)}{2(2k+1)} \int x^{k-3} A(x)B(x)dx. \end{aligned} \tag{A2}$$

In particular, if $A(x) = B(x) = {\rm Ai}(x)$, this indefinite integral simplifies to

$$\begin{aligned}\int x^k {\rm Ai}^2(x)dx &= \frac{x^{k+1}{\rm Ai}^2(x)}{2k+1} - \frac{k(k-1)x^{k-2}{\rm Ai}^2(x)}{2(2k+1)} + \frac{kx^{k-1}{\rm Ai}(x){\rm Ai}'(x)}{2k+1} \\ &\quad - \frac{x^k {\rm Ai}'^2(x)}{2k+1} + \frac{k(k-1)(k-2)}{2(2k+1)} \int x^{k-3}{\rm Ai}^2(x)dx. \end{aligned} \tag{A3}$$

Substituting this result into Equation (A1), we obtain

$$\begin{aligned}\rho_n^{\rm qm}(p) = \frac{e^{-iph_n/\hbar}}{{\rm Ai}'^2(a_n)} \sum_{k=0}^{\infty} \frac{(-ipl_g/\hbar)^k}{k!(2k+1)} \Bigg\{ &\Big[kx^{k-1}{\rm Ai}(x){\rm Ai}'(x) - x^k {\rm Ai}'^2(x) + x^{k+1}{\rm Ai}^2(x) \\ &- \frac{k(k-1)}{2} x^{k-2}{\rm Ai}^2(x)\Big]\Big|_{a_n}^{\infty} + \frac{k(k-1)(k-2)}{2} \int_{a_n}^{\infty} x^{k-3}\, {\rm Ai}^2(x)\, dx \Bigg\}. \end{aligned} \tag{A4}$$

However, since $\mathrm{Ai}(a_n) = 0$ and $\mathrm{Ai}(x) \to 0$ and $\mathrm{Ai}'(x) \to 0$ as $x \to \infty$, the above expression reduces to

$$rl\rho_n^{\mathrm{qm}}(p) = \frac{e^{-iph_n/\hbar}}{\mathrm{Ai}'^2(a_n)} \sum_{k=0}^{\infty} \frac{(-ipl_g/\hbar)^k}{k!} \left\{ \frac{a_n^k}{2k+1} \mathrm{Ai}'^2(a_n) + \frac{k(k-1)(k-2)}{2(2k+1)} \int_{a_n}^{\infty} x^{k-3} \,\mathrm{Ai}^2(x)\, dx \right\}. \tag{A5}$$

The integral in the expression above can be evaluated using the same approach. In fact, we can easily iterate the previous result. After one iteration, we obtain

$$\rho_n^{\mathrm{qm}}(p) = \frac{e^{-iph_n/\hbar}}{\mathrm{Ai}'^2(a_n)} \sum_{k=0}^{\infty} \frac{(-ipl_g/\hbar)^k}{k!} \left\{ \frac{1}{2k+1} a_n^k \mathrm{Ai}'^2(a_n) + \frac{k(k-1)(k-2)}{2(2k+1)(2k-5)} a_n^{k-3} \mathrm{Ai}'^2(a_n) + \frac{k(k-1)(k-2)(k-3)(k-4)(k-5)}{4(2k+1)(2k-5)} \int_{a_n}^{\infty} x^{k-6} \,\mathrm{Ai}^2(x)\, dx \right\}. \tag{A6}$$

As we can see, this expression is a series in inverse powers of a_n. While the second term in braces is smaller than the first by a factor of a_n^{-3}, the third is smaller than the second one by an additional factor of a_n^{-3}. One can continue iterating this result indefinitely; however, for the purposes of this paper, one can consider only the leading terms. Therefore, the asymptotic behavior of the Fourier coefficient becomes

$$\rho_n^{\mathrm{qm}}(p) \sim e^{-iph_n/\hbar} \sum_{k=0}^{\infty} \frac{(-ipl_g/\hbar)^k}{k!} \frac{1}{2k+1} \left\{ a_n^k + \frac{k(k-1)(k-2)}{2(2k-5)} a_n^{k-3} \right\}, \tag{A7}$$

which can be further simplified by defining $Q_n \equiv ph_n/\hbar$, where $h_n = -l_g a_n$. We thus obtain

$$\rho_n^{\mathrm{qm}}(p) \sim e^{-iQ_n} \left\{ \sum_{k=0}^{\infty} \frac{(iQ_n)^k}{k!(2k+1)} + \frac{1}{a_n^3} \sum_{k=0}^{\infty} \frac{(iQ_n)^k}{k!} \frac{k(k-1)(k-2)}{2(2k+1)(2k-5)} \right\}. \tag{A8}$$

We now write the Fourier coefficient as the sum of two terms, $\rho_n^{\mathrm{qm}}(p) = \rho_n^{(0)}(p) + \rho_n^{(1)}(p)$, where

$$\rho_n^{(0)}(p) = e^{-iQ_n} \sum_{k=0}^{\infty} \frac{(iQ_n)^k}{k!(2k+1)}, \quad \rho_n^{(1)}(p) = \frac{1}{a_n^3} e^{-iQ_n} \sum_{k=0}^{\infty} \frac{(iQ_n)^k}{2(k-3)!(2k+1)(2k-5)}. \tag{A9}$$

These summations can be performed in an analytical fashion and expressed in terms of special functions. For the leading term, we obtain

$$\rho_n^{(0)}(p) = e^{-iQ_n} \sqrt{\frac{\pi}{2Q_n}} \frac{1+i}{2} \,\mathrm{erf}\left(\frac{1-i}{\sqrt{2}} \sqrt{Q_n} \right), \tag{A10}$$

where $\mathrm{erf}\,(x)$ is the error function, defined as

$$\mathrm{erf}\,(x) = \frac{2}{\sqrt{\pi}} \int_0^x e^{-t^2} dt. \tag{A11}$$

The result of Equation (A10) corresponds to Equation (25) of the main text. The summation of the sub-leading term can also be evaluated analytically, with the result

$$\rho_n^{(1)}(p) = \frac{1}{96 a_n^3} \left[-\left(15 - 8iQ_n^3\right) \rho_n^{(0)}(p) + 2Q_n(2Q_n + 5i) - 15 \right], \tag{A12}$$

which corresponds to Equation (26) of the main text.

Appendix B. Validity of the Asymptotic Expression for the Quantum Fourier Coefficient

In this section, we determine the domain of validity of our asymptotic expression for the quantum Fourier coefficient. To this end, we shall compare the exact (numerically evaluated) quantum Fourier coefficient $\rho_n^{\rm qm}(p)$ given by Equation (24) versus our approximate expression $\rho_n^{\rm qm}(p) \sim \rho_n^{(0)}(p) + \rho_n^{(1)}(p)$. A simple manipulation of Equation (24) yields

$$\rho_n^{\rm qm}(p) = \frac{1}{{\rm Ai}'^2(a_n)} e^{-iQ_n} \int_{a_n}^{\infty} {\rm Ai}^2(y)\, e^{iQ_n y/a_n} dy. \tag{A13}$$

where $Q_n = ph_n/\hbar$. On the other side, the full expression for the asymptotic coefficient is $\rho_n^{\rm qm}(p) \sim \rho_n^{(0)}(p) + \rho_n^{(1)}(p)$, where

$$\rho_n^{(0)}(p) = e^{-iQ_n} \sqrt{\frac{\pi}{2Q_n}} \frac{1+i}{2} \,{\rm erf}\left(\frac{1-i}{\sqrt{2}}\sqrt{Q_n}\right), \tag{A14}$$

$$\rho_n^{(1)}(p) = \frac{1}{96 a_n^3}\Big[\Big(8iQ_n^3 - 15\Big)\rho_n^{(0)}(p) + 2Q_n(2Q_n + 5i) - 15\Big]. \tag{A15}$$

Now, in order to determine where asymptotic expression starts to deviate from the exact result in Figure A1, we plot the function $\delta\rho_n^{\rm qm}(p)$, defined as the difference between the exact result (A13) and the asymptotic result (A14) + (A15) for different values of the quantum number n. The vertical dashed lines correspond to $\pm\lambda_n$, where $\lambda_n = -a_n/2 > 0$. As we can directly see, this choice is an acceptable range for Q_n, where the quantum Fourier coefficient is well described by its asymptotic expansion. In addition, we observe that, as the quantum number increases, the approximations is better, as expected.

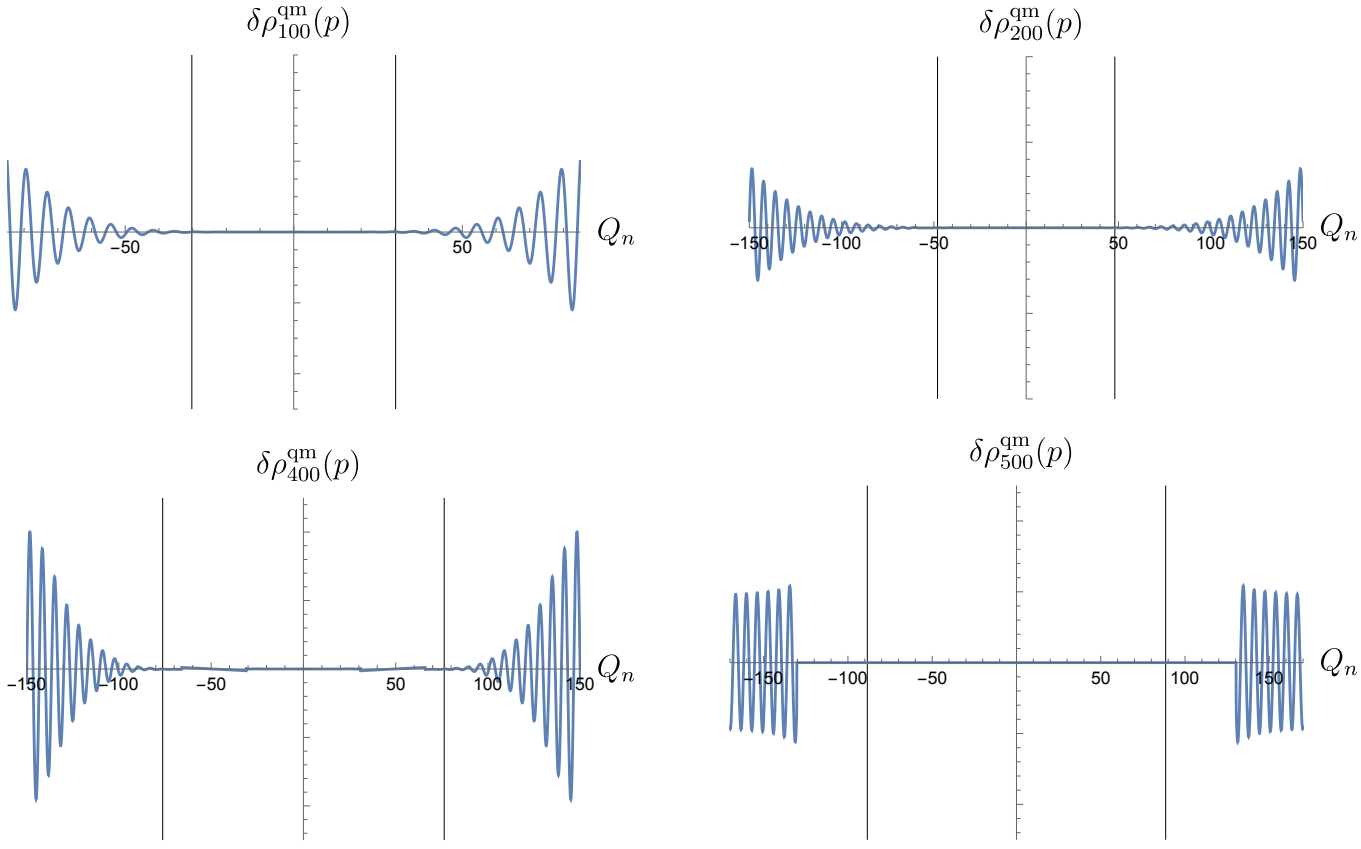

Figure A1. Difference between the exact quantum Fourier coefficient (A13) and the asymptotic result (A14) + (A15) for different values of the quantum number n. Tje vertical lines marks $\pm\lambda_n$.

References

1. Born, M. *The Born-Einstein Letters. Correspondence between Albert Einstein and Max and Hedwig Born from 1916 to 1955. With Commentaries by Max Born*; Macmillan: New York, NY, USA, 1971.
2. Ehrenfest, P. Bemerkung über die angenäherte Gültigkeit der klassischen Mechanik innerhalb der Quantenmechanik. *Z. Phys.* **1927**, *45*, 455–457. [CrossRef]
3. Feynman, R.; Hibbs, A.; Styer, D. *Quantum Mechanics and Path Integrals*; Dover Books on Physics, Dover Publications: New York, NY, USA, 2010.
4. Brillouin, L. La mécanique ondulatoire de Schrödinger; une méthode générale de resolution par approximations successives. *Compt. Rend. Hebd. Seances Acad. Sci.* **1926**, *183*, 24–26.
5. Kramers, H.A. Wellenmechanik und halbzahlige Quantisierung. *Z. Phys.* **1926**, *39*, 828–840. [CrossRef]
6. Wentzel, G. Eine Verallgemeinerung der Quantenbedingungen für die Zwecke der Wellenmechanik. *Z. Phys.* **1926**, *38*, 518–529. [CrossRef]
7. Makowski, A.J. A brief survey of various formulations of the correspondence principle. *Eur. J. Phys.* **2006**, *27*, 1133–1139. [CrossRef]
8. Liboff, R.L. The correspondence principle revisited. *Phys. Today* **1984**, *37*, 50–55. [CrossRef]
9. Cañas, J.A.; Bernal, J.; Martín-Ruiz, A. Exact classical limit of the quantum bouncer. *Eur. Phys. J. Plus* **2022**, *137*. [CrossRef]
10. Curtright, T.L.; Fairlie, D.B.; Zachos, C.K. *A Concise Treatise on Quantum Mechanics in Phase Space*; World Scientific: Singapore, 2014. [CrossRef]
11. Mostowski, J.; Pietraszewicz, J. Wigner Function for Harmonic Oscillator and The Classical Limit. *arXiv* **2021**, arXiv:2104.06638.
12. Shin, G.R.; Rafelski, J. Relativistic classical limit of quantum theory. *Phys. Rev.* **1993**, *48*, 1869–1874. [CrossRef]
13. Litim, D.F.; Manuel, C. Semi-classical transport theory for non-Abelian plasmas. *Phys. Rep.* **2002**, *364*, 451–539. [CrossRef]
14. Mari, A.; Eisert, J. Positive Wigner Functions Render Classical Simulation of Quantum Computation Efficient. *Phys. Rev. Lett.* **2012**, *109*, 230503. [CrossRef] [PubMed]
15. Robinett, R.W. Quantum and classical probability distributions for position and momentum. *Am. J. Phys.* **1995**, *63*, 823–832. [CrossRef]
16. Yoder, G.W. Using classical probability functions to illuminate the relation between classical and quantum physics. *Am. J. Phys.* **2006**, *74*, 404–411. [CrossRef]
17. Robinett, R.W. Visualizing classical and quantum probability densities for momentum using variations on familiar one-dimensional potentials. *Eur. J. Phys.* **2002**, *23*, 165–174. [CrossRef]
18. Robinett, R.W. Visualizing the solutions for the circular infinite well in quantum and classical mechanics. *Am. J. Phys.* **1996**, *64*, 440–446. [CrossRef]
19. Doncheski, M.A.; Robinett, R.W. Comparing classical and quantum probability distributions for an asymmetric infinite well. *Eur. J. Phys.* **2000**, *21*, 217–228. [CrossRef]
20. Bernal, J.; Martín-Ruiz, A.; García-Melgarejo, J.C. A Simple Mathematical Formulation of the Correspondence Principle. *J. Mod. Phys.* **2013**, *4*, 108–112. [CrossRef]
21. Martín-Ruiz, A.; Bernal, J.; Carbajal-Domínguez, A. Macroscopic Quantum Behaviour of Periodic Quantum Systems. *J. Mod. Phys.* **2014**, *5*, 44–50. [CrossRef]
22. Martín-Ruiz, A.; Bernal, J.; Frank, A.; Carbajal-Dominguez, A. The Classical Limit of the Quantum Kepler Problem. *J. Mod. Phys.* **2013**, *4*, 818–822. [CrossRef]
23. Hernandez, K.G.; Aguilar-Gutierrez, S.E.; Bernal, J. On the correspondence principle for the Klein-Gordon and Dirac Equations. *J. Theor. Appl. Phys.* **2023**, *16*. [CrossRef]
24. Wald, R. *General Relativity*; University of Chicago Press: Chicago, IL, USA, 2010.
25. Cañas, J.A.; Bernal, J.; Martín-Ruiz, A. Testing the equivalence principle with time-diffracted free-falling quantum particles. *Eur. Phys. J. Plus* **2022**, *137*. [CrossRef]
26. v. Eötvös, R.; Pekár, D.; Fekete, E. Beiträge zum gesetze der proportionalität von trägheit und gravität. *Ann. Phys.* **1922**, *373*, 11–66. [CrossRef]
27. Will, C.M. The Confrontation between General Relativity and Experiment. *Living Rev. Relativ.* **2014**, *17*, 1–117. [CrossRef] [PubMed]
28. Touboul, P.; Métris, G.; Rodrigues, M.; Bergé, J.; Robert, A.; Baghi, Q.; André, Y.; Bedouet, J.; Boulanger, D.; Bremer, S.; et al. *MICROSCOPE* Mission: Final Results of the Test of the Equivalence Principle. *Phys. Rev. Lett.* **2022**, *129*, 121102. [CrossRef] [PubMed]
29. Orlando, P.J.; Mann, R.B.; Modi, K.; Pollock, F.A. A test of the equivalence principle(s) for quantum superpositions. *Class. Quantum Gravity* **2016**, *33*, 19LT01. [CrossRef]
30. Rosi, G.; D'Amico, G.; Cacciapuoti, L.; Sorrentino, F.; Prevedelli, M.; Zych, M.; Brukner, Č.; Tino, G.M. Quantum test of the equivalence principle for atoms in coherent superposition of internal energy states. *Nat. Commun.* **2017**, *8*, 15529. [CrossRef]
31. Albers, H.; Herbst, A.; Richardson, L.L.; Heine, H.; Nath, D.; Hartwig, J.; Schubert.; Woltmann, M.; Lämmerzahl, C.; Herrmann, S.; et al. Quantum test of the Universality of Free Fall using rubidium and potassium. *Eur. Phys. J.* **2020**, *74*, 145. [CrossRef]

32. Struckmann, C.; Corgier, R.; Loriani, S.; Kleinsteinberg, G.; Gox, N.; Giese, E.; Métris, G.; Gaaloul, N.; Wolf, P. Platform and environment requirements of a satellite quantum test of the weak equivalence principle at the 10^{-17} level. *Phys. Rev. D* **2024**, *109*, 064010. [CrossRef]
33. Flores, P.C.M.; Galapon, E.A. Quantum free-fall motion and quantum violation of the weak equivalence principle. *Phys. Rev.* **2019**, *99*, 042113. [CrossRef]
34. Davies, P.C.W. Quantum mechanics and the equivalence principle. *Class. Quantum Gravity* **2004**, *21*, 2761–2772. [CrossRef]
35. Zych, M.; Brukner, Č. Quantum formulation of the Einstein equivalence principle. *Nat. Phys.* **2018**, *14*, 1027–1031. [CrossRef]
36. Seveso, L.; Paris, M.G. Can quantum probes satisfy the weak equivalence principle? *Ann. Phys.* **2017**, *380*, 213–223. [CrossRef]
37. Okon, E.; Callender, C. Does quantum mechanics clash with the equivalence principle—And does it matter? *Eur. J. Philos. Sci.* **2010**, *1*, 133–145. [CrossRef]
38. Durrett, R. *Probability: Theory and Examples*, 2nd ed.; Duxbury Press: Belmont, CA, USA, 1996.
39. Leon-Garcia, A. *Probability, Statistics, and Random Processes for Electrical Engineering*, 3rd ed.; Pearson/Prentice Hall: Upper Saddle River, NJ, USA, 2008.
40. Marks, R.J., II. *Handbook of Fourier Analysis & Its Applications*; Oxford University Press:Oxford, UK, 2009. [CrossRef]
41. Kouznetsov, D.; Oberst, H.; Neumann, A.; Kuznetsova, Y.; Shimizu, K.; Bisson, J.F.; Ueda, K.; Brueck, S.R.J. Ridged atomic mirrors and atomic nanoscope. *J. Phys. At. Mol. Opt. Phys.* **2006**, *39*, 1605–1623. [CrossRef]
42. Abramowitz, M.; Stegun, I. *Handbook of Mathematical Functions: With Formulas, Graphs, and Mathematical Tables*; Applied mathematics series; Dover Publications: New York, NY, USA, 1965.
43. Gibbs, R.L. The quantum bouncer. *Am. J. Phys.* **1975**, *43*, 25–28. [CrossRef]
44. Nesvizhevsky, V.V.; Börner, H.G.; Petukhov, A.K.; Abele, H.; Baeßler, S.; Rueß, F.J.; Stöferle, T.; Westphal, A.; Gagarski, A.M.; Petrov, G.A.; et al. Quantum states of neutrons in the Earth's gravitational field. *Nature* **2002**, *415*, 297–299. [CrossRef]
45. Abele, H.; Cronenberg, G.; Geltenbort, P.; Jenke, T.; Lins, T.; Saul, H. qBounce, the Quantum Bouncing Ball Experiment. *Phys. Procedia* **2011**, *17*, 4–9. [CrossRef]
46. Vezhlev, E.O.; Voronin, V.V.; Kuznetsov, I.A.; Semenikhin, S.Y.; Fedorov, V.V. Verification of the weak equivalence principle with Laue diffracting neutrons: Test experiment. *Phys. Part. Nucl. Lett.* **2013**, *10*, 357–360. [CrossRef]
47. Goodings, D.; Szeredi, T. The quantum bouncer by the path integral method. *Am. J. Phys.* **1991**, *59*, 924–930. [CrossRef]
48. Gea-Banacloche, J. A quantum bouncing ball. *Am. J. Phys.* **1999**, *67*, 776–782. [CrossRef]
49. Martín-Ruiz, A.; Frank, A.; Urrutia, L. Analysis of the quantum bouncer using polymer quantization. *Phys. Rev.* **2015**, *92*, 045018. [CrossRef]
50. Vallé, O.; Soares, M. *Airy Functions and Applications to Physics*, 2nd ed.; Imperial College Press: London, UK, 2010. [CrossRef]